

Autonomous In-motion Alignment for Land Vehicle Strapdown Inertial Navigation System without the Aid of External Sensors

Qiangwen Fu, Yang Liu, Zhenbo Liu, Sihai Li and Bofan Guan

(School of Automation, Northwestern Polytechnical University, China)

(E-mail: fuqiangwen@nwpu.edu.cn)

This paper describes a fully autonomous real-time in-motion alignment algorithm for Strapdown Inertial Navigation Systems (SINS) in land vehicle applications. Once the initial position is available, the vehicle can start a mission immediately with accurate attitude, position and velocity information determined within ten minutes. This is achieved by two tightly coupled stages, that is, real-time Double-vector Attitude Determination Coarse Alignment (DADCA) and Backtracking Fine Alignment (BFA). In the DADCA process, the vehicle motion is omitted to roughly estimate the attitude at the very start of the alignment. Meanwhile, attitude quaternions and velocity increments are extracted and recorded. The BFA process utilises the stored data and exploits the Non-Holonomic Constraints (NHC) of a vehicle to obtain virtual velocity measurements. A linear SINS/NHC Kalman filter with mounting angles as extended states is constructed to improve the fine alignment accuracy. The method is verified by three vehicle tests, which shows that the accuracy of alignment azimuth is 0.0358° (Root Mean Square, RMS) and the positioning accuracy is about 15 m (RMS) at the end of the alignment.

KEY WORDS

1. In-motion alignment.
2. Backtracking navigation.
3. Non-Holonomic Constraints (NHC).
4. Land navigation.

Submitted: 28 December 2017. Accepted: 21 May 2018. First published online: 29 June 2018.

1. INTRODUCTION. As a dead-reckoning navigation method, the Strapdown Inertial Navigation System (SINS) can track the attitude, velocity and position of a vehicle by numerical integration of the inertial sensors' measurements (Titterton and Weston, 2004). To establish the initial value for integration, the SINS initial alignment process is of great importance because it will largely determine the subsequent navigation accuracy (Li et al., 2013a). Traditional initial alignment methods, usually consisting of coarse-alignment and fine-alignment stages, must be completed prior to vehicle movement (Savage, 2000). Typically, the coarse-alignment phase is required to estimate the vehicle's heading to

an accuracy of a few degrees and pitch/roll to a few tenths of a degree to allow the fine-alignment filter to operate in its linear region (Silson, 2011). There are two obvious limitations in traditional alignment methods: firstly, keeping a vehicle stationary for alignment consumes time and space (Liu et al., 2014; Wang et al., 2012; Shin and El-Sheimy, 2004), and can be dangerous on the battlefield where high manoeuvrability is required and secondly, the coarse-alignment phase consumes a certain period of time (typically 30 to 120 seconds) (Hu and Cheng, 2014) but has no direct contribution to final alignment accuracy.

Handling the first limitation is particularly important for military applications. In order to enhance manoeuvrability and thus survivability, it is necessary to achieve high accuracy alignment within a short time whether the vehicle is static or moving. Many efforts have been devoted to high-accuracy in-motion alignment techniques, which always need external sensors to compensate the vehicle motions. A Global Navigation Satellite Systems (GNSS), most frequently the Global Positioning System (GPS), providing velocity and position directly in the geographic coordinate system, is widely used as an aiding source for in-motion alignment (Jiang et al., 2013; Kaygısız and Sen, 2015; Kubo et al., 2006; Wu and Pan, 2013a; 2013b). However, GNSS are vulnerable to jamming, blocking and spoofing, greatly affecting their availability and reliability (Chang et al., 2016; Pan and Wu, 2016; Liu et al., 2018). For the land vehicles of interest here, an odometer is the most commonly used velocity-aiding source for autonomous initial alignment (Xu et al., 2017; Bimal and Joshi, 2015; Wu, 2014). Since an odometer provides velocity along the vehicle body frame, odometer-aided in-motion alignment usually requires not only attitude determination but also velocity and position calculation (Chang et al., 2017). The existing odometer-aided alignment methods fall into three main categories: (1) nonlinear Kalman filter approaches (Bimal and Joshi, 2015; Wu, 2014; Chang et al., 2017; Li et al., 2013b), which can tolerate a large initial misalignment angle and allow the vehicle to move without a stationary period, but suffer from redundant computation; (2) linear Kalman filter INS/odometer integration, which can easily achieve attitude, velocity and position in the alignment, while the only shortcoming lies in that a 30 to 120 seconds stationary period is still needed for coarse alignment; (3) multi-vector attitude determination in an inertial frame, which has been the most popular method over the last decade (Chang et al., 2016; Jiang et al., 2013; Wu, 2014), but the mounting angles and odometer's scale factor must be calibrated perfectly in advance to ensure attitude and position alignment accuracy, and the heading alignment result may deteriorate by the equivalent change rate of acceleration bias caused by a possible turn of the vehicle.

For the second limitation, a backtracking navigation scheme is a good solution to take full use of the coarse alignment time. The method uses the inertial frame alignment strategy as forward coarse alignment, followed by backtracking linear Kalman filter fine alignment based on the data computed in the coarse alignment process (Li et al., 2014; 2013c). In order to avoid the overshoot caused by error model switch, the traditional backtracking scheme and subsequent navigation is established in the inertial frame instead of the classical geographic frame (Li et al., 2014). As a non-local level frame mechanisation, navigation in the inertial frame cannot conform to land navigation usage habits and will bring new problems. The unstable height channel cannot be decoupled in the inertial frame, so the navigation results in all three channels will be contaminated, and it is also difficult to damp the altitude divergence by other sensors such as an atmospheric pressure altimeter.

In Dissanayake et al. (1999), a real time, on-the-fly, roll and pitch alignment algorithm for SINS on land vehicles without external sensors was proposed, which was achieved by exploiting the Non-Holonomic Constraints (NHC) that govern the motion of a vehicle on a surface. Focusing on a low-accuracy Inertial Measurement Unit (IMU), this study does not take the heading alignment and mounting angles into account, so the positioning accuracy is limited. Inspired by Dissanayake et al. (1999), we propose a novel in-motion alignment method based on NHC and a backtracking navigation scheme for land vehicles. The proposed method consists of two tightly coupled stages. First, in the coarse alignment process, double-vector attitude determination based on a second-order integral of specific force in the inertial frame is deduced, to approximately estimate the attitude at the very start of the alignment. Meanwhile, attitude quaternions and velocity increments are extracted and recorded with lower frequency. Second, the backtracking process uses the estimated initial attitude and stored data to accomplish the fine alignment by SINS/NHC integrated navigation based on a linear Kalman filter in the geographic coordinate system. The proposed method has several advantages as follows:

- (1) The alignment can be accomplished autonomously without any external sensors except the initial position. The mounting angles can be automatically estimated, and the pre-calibration process is unnecessary.
- (2) There is no need to keep a vehicle stationary for coarse alignment, allowing the vehicle to move once the initial position is available. All inertial sensor data are used in both coarse alignment and fine alignment, and it is equivalent to lengthening the alignment time which contributes to improvement of the alignment accuracy.
- (3) The method cannot only align the attitude to high accuracy within limited time, but also determines the velocity and position with satisfactory accuracy at the end of the alignment.
- (4) Without large storage or redundant computation such as nonlinear filters, this scheme is easy to use in real time applications. The backtracking fine alignment and subsequent navigation arranged in the geographic frame are convenient for practical land vehicle applications.

The rest of this paper is organised as follows. Section 2 describes the proposed in-motion alignment algorithm, including the overall alignment strategy, coarse alignment process in the inertial frame, backtracking navigation updating and SINS/NHC integrated fine alignment process. Section 3 presents the results and discussions of three land vehicle in-motion alignment tests. Conclusions are drawn in Section 4.

2. PROPOSED ALIGNMENT ALGORITHM. In this paper, basic coordinate systems are defined as follows: the local level East-North-Up (ENU) geographic coordinate is chosen as the navigation frame, denoted by n -frame. The IMU b -frame is implicitly predefined by the sensitive axes of inertial sensors with axes pointing right, forward, and upward, respectively. The e -frame denotes the Earth-Centred Earth-Fixed (ECEF) reference frame, and the m -frame is the vehicle frame aligned with right-forward-up vehicle body axes.

2.1. In-motion alignment scheme. At the very start of alignment, the vehicle is static, and the initial velocity can be regarded as zero. Once an initial position is available, the SINS can start alignment and the vehicle is allowed to move immediately without a requirement for a specified stationary time. In order to accomplish accurate in-motion alignment

DADCA process is to determine the initial constant matrix $C_{b_0}^{n_0}$ instead of the time-varying attitude matrix $C_b^n(t)$.

The navigation specific force equation in the n -frame is well known as (Qin, 2014):

$$\dot{\mathbf{v}}^n = C_b^n \mathbf{f}^b - (2\boldsymbol{\omega}_{ie}^n + \boldsymbol{\omega}_{en}^n) \times \mathbf{v}^n + \mathbf{g}^n \tag{2}$$

where \mathbf{v}^n denotes the velocity relative to the Earth in the n -frame, \mathbf{f}^b is the specific force in the b -frame, $\boldsymbol{\omega}_{ie}^n$ is the Earth rotation rate vector in the n -frame, $\boldsymbol{\omega}_{en}^n$ is the angular rate of the n -frame with respect to the e -frame and \mathbf{g}^n is the gravity vector.

Using Equation (1), Equation (2) can be reorganised as:

$$C_n^{n_0} [\mathbf{g}^n - \dot{\mathbf{v}}^n - (2\boldsymbol{\omega}_{ie}^n + \boldsymbol{\omega}_{en}^n) \times \mathbf{v}^n] = -C_{b_0}^{n_0} (C_b^{b_0} \mathbf{f}^b) \tag{3}$$

Without the external velocity and position information required for traditional in-motion coarse alignment, the in-motion alignment is simplified as a stationary alignment. It is equivalent to ignoring the part $-\dot{\mathbf{v}}^n - (2\boldsymbol{\omega}_{ie}^n + \boldsymbol{\omega}_{en}^n) \times \mathbf{v}^n$ on the left-hand side of Equation (3). Even though many error sources will be introduced, such a simplification is an expedient without auxiliary sensors. Denoting the current time as t , we have:

$$\mathbf{g}^{n_0}(t) = -C_{b_0}^{n_0} \tilde{\mathbf{f}}^{b_0}(t) \tag{4}$$

in which:

$$\mathbf{g}^{n_0}(t) = C_n^{n_0}(t) \mathbf{g}^n \tag{5}$$

$$\tilde{\mathbf{f}}^{b_0}(t) = C_b^{b_0}(t) \tilde{\mathbf{f}}^b(t) \tag{6}$$

where $\tilde{\mathbf{f}}^b(t)$ is the specific force measured by accelerometers in the b -frame, $C_n^{n_0}(t)$ denotes the changes of the n -frame during the alignment process and can be calculated as:

$$C_n^{n_0}(t) = C_e^n(t) C_{e_0}^e(t) C_{n_0}^{e_0} \tag{7}$$

with

$$C_{n_0}^{e_0} = \begin{bmatrix} 0 & -\sin L_0 & \cos L_0 \\ 1 & 0 & 0 \\ 0 & \cos L_0 & \sin L_0 \end{bmatrix}, C_{e_0}^e(t) = \begin{bmatrix} \cos \omega_{ie} t & \sin \omega_{ie} t & 0 \\ -\sin \omega_{ie} t & \cos \omega_{ie} t & 0 \\ 0 & 0 & 1 \end{bmatrix} \text{ and } C_e^n(t) = (C_{n_0}^{e_0})^T$$

where ω_{ie} denotes the magnitude of the Earth rotation rate and L_0 the initial geographic latitude.

In Equation (6), $C_b^{b_0}(t)$ represents the orientation of the b_0 -frame relative to the b -frame and can be calculated as:

$$\dot{C}_b^{b_0}(t) = C_b^{b_0}(t) (\tilde{\boldsymbol{\omega}}_{ib}^b \times) \tag{8}$$

where $\tilde{\boldsymbol{\omega}}_{ib}^b$ denotes the body angular rate measured by gyroscopes in b -frame, and the skew symmetric matrix $(\cdot \times)$ is defined so that the cross product satisfies $\mathbf{a} \times \mathbf{b} = (\mathbf{a} \times) \mathbf{b}$ for two arbitrary vectors (Wu and Pan, 2013b).

The alternative of Equation (8) is the quaternion differential equation:

$$\dot{\mathbf{Q}}_b^{b_0}(t) = \frac{1}{2} \mathbf{Q}_b^{b_0}(t) \otimes \tilde{\boldsymbol{\omega}}_{ib}^b \tag{9}$$

where \otimes denotes the quaternion product and the initial condition is $\mathbf{Q}_b^{b_0}(0) = [1 \ 0 \ 0 \ 0]^T$.

Since the initial attitude matrix $C_{b_0}^{n_0}$ is constant, it can be determined by a Three-axis Attitude Determination-based (TRIAD) algorithm with two non-collinear vectors (James, 2012; Jiang, 1998). It is obvious from Equation (4) that the vectors of $\mathbf{g}^{n_0}(t)$ and $\tilde{\mathbf{f}}^{b_0}(t)$ at different moments are suitable for analytic alignment. Moreover, in order to suppress the influence of vehicle motion disturbance, a second-order integration method is introduced to accomplish coarse alignment as follows

$$C_{b_0}^{n_0} = \begin{bmatrix} (\mathbf{p}_{t_1}^{n_0})^T \\ (\mathbf{p}_{t_1}^{n_0} \times \mathbf{p}_{t_2}^{n_0})^T \\ (\mathbf{p}_{t_1}^{n_0} \times \mathbf{p}_{t_2}^{n_0} \times \mathbf{p}_{t_1}^{n_0})^T \end{bmatrix}^{-1} \begin{bmatrix} (\tilde{\mathbf{p}}_{t_1}^{b_0})^T \\ (\tilde{\mathbf{p}}_{t_1}^{b_0} \times \tilde{\mathbf{p}}_{t_2}^{b_0})^T \\ (\tilde{\mathbf{p}}_{t_1}^{b_0} \times \tilde{\mathbf{p}}_{t_2}^{b_0} \times \tilde{\mathbf{p}}_{t_1}^{b_0})^T \end{bmatrix} \tag{10}$$

with

$$\begin{aligned} \tilde{\mathbf{p}}_{t_1}^{b_0} &= \int_0^{t_1} \int_0^t C_b^{b_0}(t) \tilde{\mathbf{f}}^b(t) d\tau dt, & \tilde{\mathbf{p}}_{t_2}^{b_0} &= \int_0^{t_2} \int_0^t C_b^{b_0}(t) \tilde{\mathbf{f}}^b(t) d\tau dt, \\ \tilde{\mathbf{p}}_{t_1}^{n_0} &= \int_0^{t_1} \int_0^t C_n^{n_0}(t) \mathbf{g}^n d\tau dt, & \tilde{\mathbf{p}}_{t_2}^{n_0} &= \int_0^{t_2} \int_0^t C_n^{n_0}(t) \mathbf{g}^n d\tau dt, \end{aligned}$$

where t_1 and t_2 are selected as $t_2 = t_c, t_1 = t_2/2$.

From Equation (10), the initial matrix can be approximately obtained, and one of the main error sources comes from the assumption of stationary alignment. The misalignment of the initial attitude caused by ignoring the motion acceleration in Equation (3) is approximately equal to the gravity deflection associated with the travelled distance. Since the normal speed of a land vehicle is generally less than 35 m/s and the alignment time lasts less than 10 minutes, it is possible to align the initial attitude to an accuracy of several degrees.

2.2.2. *Data record for BFA.* During the real time DADCA process, attitude quaternion and velocity increments must be recorded for the BFA process. To reduce storage space and computation load, the required data should be extracted and recorded with a lower frequency such as 1 Hz, which is the same as the Kalman filter measurement update frequency in the subsequent BFA process. In summary, seven floating-point data should be recorded in every storage cycle including four-dimensional attitude quaternion $\mathbf{Q}_{b_k}^{b_0}$ and three-dimensional velocity increments $\Delta \tilde{\mathbf{v}}_k^{b_0}$. Note that the quaternion instead of the attitude matrix should be stored to reduce the data volume. The quaternion $\mathbf{Q}_{b_k}^{b_0}$ can be obtained from Equation (9), and the velocity increments can be calculated as

$$\Delta \tilde{\mathbf{v}}_k^{b_0} = \int_{t_{k-1}}^{t_k} C_b^{b_0}(t) \tilde{\mathbf{f}}^b(t) dt \tag{11}$$

where the integral time interval $[t_{k-1}, t_k]$ is the same as the recording cycle, that is, one second in this paper. Given that the alignment time is 600 seconds, only 4,200 floating-point data additional storage space is needed, which can be easily afforded by ordinary SINS navigation computers.

2.3. *The BFA process.*

2.3.1. *Backtracking navigation update.* Besides the initial velocity and position, the approximate initial attitude matrix $C_{b_0}^{n_0}$ is available after the DADCA process, so the navigation parameters through the whole alignment process can be calculated based on backtracking navigation with the stored data. As the normal inertial navigation solution, the backtracking navigation includes attitude, velocity and position updates.

2.3.1.1. *Backtracking attitude update.* The time-varying attitude matrix, $C_{b_k}^{n_k}$ which represents the orientation of the n -frame relative to the b -frame at time t_k , can be calculated as follows:

$$C_{b_k}^{n_k} = C_{n_0}^{n_k} C_{b_0}^{n_0} C_{b_k}^{b_0} \tag{12}$$

where $C_{b_0}^{n_0}$ is the alignment result of the DADCA process, and $C_{b_k}^{b_0}$ can easily be converted from the stored quaternion $Q_{b_k}^{b_0}$ (Titterton and Weston, 2004). As the current position is available, the calculation of the matrix $C_{n_0}^{n_k}$ in the BFA process is somewhat different to Equation (7):

$$C_{n_0}^{n_k} = C_{e_k}^{n_k} C_{e_0}^{e_k} C_{n_0}^{e_0} \tag{13}$$

while $C_{n_0}^{e_0}$ is calculated the same way as in Equation (7), $C_{e_k}^{n_k}$ and $C_{e_0}^{e_k}$ are obtained as:

$$C_{e_k}^{n_k} = \begin{bmatrix} 0 & 1 & 0 \\ -\sin L_k & 0 & \cos L_k \\ \cos L_k & 0 & \sin L_k \end{bmatrix}, C_{e_0}^{e_k} = \begin{bmatrix} \cos \Delta & \sin \Delta & 0 \\ -\sin \Delta & \cos \Delta & 0 \\ 0 & 0 & 1 \end{bmatrix}$$

where $\Delta = \lambda_k - \lambda_0 + \omega_{ie}t$ and λ_0 denotes the initial geographic longitude at time $t = 0$. λ_k and L_k denotes the current longitude and latitude at time t_k .

Although the backtracking attitude update is not explicitly used in subsequent velocity and position updates, it is required to solve the state Equation (24) and the measurement Equations (25)–(26) in the backtracking SINS/NHC Kalman filter. Meanwhile, the corrected attitude result should be obtained as:

$$\hat{C}_{b_k}^{n_k} = [I + (\hat{\phi}^n \times)] C_{b_k}^{n_k} \tag{14}$$

where $\hat{\phi}^n$ denotes the attitude misalignment angles estimated in fine alignment.

2.3.1.2. *Backtracking velocity update.* The velocity in the n -frame is updated as follows:

$$v_k^n = v_{k-1}^n + C_{n_{k-1}}^{n_{k-1/2}} C_{n_0}^{n_{k-1}} C_{b_0}^{n_0} \Delta v_k^{b_0} - (2\omega_{ie,k-1}^n + \omega_{en,k-1}^n) \times v_{k-1}^n T_s + g_{k-1}^n T_s \tag{15}$$

where the subscript k denotes the parameter of the current update cycle and $k - 1$ is the last update cycle, so v_k^n and v_{k-1}^n denote the velocity at the current and last cycle, respectively. $C_{n_0}^{n_{k-1}}$ can be obtained by Equation (13), $\Delta v_k^{b_0}$ is the stored velocity increments in the b_0 -frame, and $T_s = 1$ s denotes the one second update cycle. Since ω_{in}^n changes slowly, it is reasonable to approximate the attitude matrix by $C_{n_{k-1}}^{n_{k-1/2}} \approx I + (\Phi_{k/2}^n \times)$, where $\Phi_{k/2}^n \approx -1/2(\omega_{ie,k-1}^n + \omega_{en,k-1}^n)T_s$ denotes the n -frame rotation vector from t_{k-1} to $t_{k-1} + T_s/2$.

2.3.1.3. *Backtracking position update.* Given that the velocity is obtained, the position $[\lambda, L, h]^T$ can be updated as

$$\begin{bmatrix} \lambda_k \\ L_k \\ h_k \end{bmatrix} = \begin{bmatrix} \lambda_{k-1} \\ L_{k-1} \\ h_{k-1} \end{bmatrix} + \frac{1}{2} R^c (v_{k-1}^n + v_k^n) T_s \tag{16}$$

$$R^c = \begin{bmatrix} 1/[(R_N + h) \cos L_{k-1}] & 0 & 0 \\ 0 & 1/(R_M + h) & 0 \\ 0 & 0 & 1 \end{bmatrix} \tag{17}$$

where R_N and R_M are the transverse and meridian radius of curvature, respectively.

2.3.2. *Fine alignment algorithm.* Since the backtracking navigation is conducted in the n -frame instead of the inertial frame, it is easy to adopt the well-known non-holonomic constraints to improve the fine alignment accuracy. Unlike an air vehicle, the motion of a wheeled vehicle on the land surface is governed by two non-holonomic constraints. When the vehicle does not jump off or slide on the ground, velocity of the vehicle in the plane perpendicular to the forward direction is zero, which is a virtual two-dimensional velocity measurement. Under ideal conditions, there is no side slip along the direction of the rear axle and no motion normal to the road surface, the constraints are (Dissanayake et al., 2001):

$$\begin{cases} v_x^m = 0 \\ v_z^m = 0 \end{cases} \tag{18}$$

In practical situations, these constraints are somewhat violated due to the presence of side slip during cornering and vibrations caused by the engine and suspension system. Approximately, it is possible to model the extent of such violations as Gaussian white noise with zero mean and variance σ_x^2 and σ_z^2 , respectively (Dissanayake et al., 2001).

The SINS/NHC integrated navigation based on Kalman filter is a good solution to realise the in-motion fine alignment without external sensors. In practice, the mounting angles between the IMU and the vehicle will noticeably affect the position accuracy, and they are commonly treated as main error sources to be estimated in SINS/odometer integrated vehicle navigation (Wu, 2014). However, for pure SINS/NHC navigation, which is often used to aid a low-cost SINS during GNSS signal blockages, the mounting angles are usually ignored (Dissanayake et al., 2001; Peng et al., 2013; Rothman et al., 2015). Taking the mounting angles into the error state vector of the SINS/NHC Kalman filter to be estimated, we have realised a high positioning accuracy of horizontal error to 16.6 m Circular Error Probability (CEP) and vertical error 14.9 m Probable Error (PE) with a navigation-grade SINS in an 80 km vehicle test (Fu et al., 2012).

Since the mounting angles are inevitable and non-negligible for high-accuracy positioning, they should be handled properly in the SINS/NHC integration. The velocity of the vehicle calculated by SINS can be converted to the m -frame as (Wu, 2014):

$$\tilde{\mathbf{v}}_I^m = \tilde{\mathbf{C}}_b^m \tilde{\mathbf{C}}_n^b \tilde{\mathbf{v}}_I^n \tag{19}$$

where $\tilde{\mathbf{C}}_b^m$ denotes the converted matrix formed by the three mounting angles, and $\tilde{\mathbf{C}}_n^b$ and $\tilde{\mathbf{v}}_I^n$ are the attitude matrix and velocity calculated by SINS, respectively.

In general, the mounting angles can be easily controlled to small angles, and the converted matrix $\tilde{\mathbf{C}}_b^m$ approximately satisfies:

$$\tilde{\mathbf{C}}_b^m \approx \mathbf{I} + \boldsymbol{\alpha} \times \tag{20}$$

where $\boldsymbol{\alpha} = [\alpha_x \ \alpha_y \ \alpha_z]^T$ denotes the three-dimensional mounting angle vector.

Considering the navigation errors of SINS and the non-holonomic constraints, Equation (19) can be rewritten as (Fu et al., 2012):

$$\begin{aligned}
 \tilde{\mathbf{v}}_I^m &= (\mathbf{I} + \boldsymbol{\alpha} \times) \mathbf{C}_n^b (\mathbf{I} + \boldsymbol{\phi}^n \times) (\mathbf{v}^n + \delta \mathbf{v}_I^n) \\
 &\approx \mathbf{v}^m + \mathbf{C}_n^b \delta \mathbf{v}_I^n - \mathbf{C}_n^b (\mathbf{v}^n \times) \boldsymbol{\phi}^n - (\mathbf{C}_n^b \mathbf{v}^n) \times \boldsymbol{\alpha} \\
 &\approx \mathbf{v}^m + \mathbf{C}_n^b \delta \mathbf{v}_I^n - \mathbf{C}_n^b (\mathbf{v}^n \times) \boldsymbol{\phi}^n - \begin{bmatrix} 0 & 0 & v_y^m \\ 0 & 0 & 0 \\ -v_y^m & 0 & 0 \end{bmatrix} \times \begin{bmatrix} \alpha_x \\ \alpha_y \\ \alpha_z \end{bmatrix}
 \end{aligned} \tag{21}$$

where $\boldsymbol{\phi}^n = [\phi_E, \phi_N, \phi_U]^T$ and $\delta \mathbf{v}_I^n = [\delta v_E, \delta v_N, \delta v_U]^T$ represent the attitude misalignment angle and velocity error vector, respectively.

It is obvious that the roll mounting angle α_y is totally irrelevant to the vehicular velocity $\tilde{\mathbf{v}}_I^m$, so it is an unobservable error state and should be disregarded in the SINS/NHC Kalman filter. The other two mounting angles α_x and α_z can be treated as unknown random constants which satisfy:

$$\begin{cases} \dot{\alpha}_x = 0 \\ \dot{\alpha}_z = 0 \end{cases} \tag{22}$$

Combining the error model of SINS and the mounting angles, the 17-dimensional error state vector of SINS/NHC integration can be defined as:

$$\mathbf{x}(t) = [(\boldsymbol{\phi}^n)^T \quad (\delta \mathbf{v}_I^n)^T \quad (\delta \mathbf{P})^T \quad (\boldsymbol{\epsilon}^b)^T \quad (\boldsymbol{\nabla}^b)^T \quad \alpha_x \quad \alpha_z]^T \tag{23}$$

where $\delta \mathbf{P} = [\delta \lambda, \delta L, \delta h]^T$ denotes the position errors, $\boldsymbol{\epsilon}^b$ and $\boldsymbol{\nabla}^b$ denote the gyro and accelerometer biases, respectively.

The corresponding system equation of the error-state Kalman filter is:

$$\dot{\mathbf{x}}(t) = \begin{bmatrix} \mathbf{F}_{\text{INS}} & \mathbf{0}_{15 \times 2} \\ \mathbf{0}_{2 \times 15} & \mathbf{0}_{2 \times 2} \end{bmatrix} \mathbf{x}(t) + \begin{bmatrix} -\mathbf{C}_b^n \boldsymbol{\epsilon}_w^b \\ \mathbf{C}_b^n \boldsymbol{\nabla}_w^b \\ \mathbf{0}_{11 \times 1} \end{bmatrix} \tag{24}$$

where \mathbf{F}_{INS} is the 15×15 state transition matrix based on typical SINS error model (Qin, 2013), $\boldsymbol{\epsilon}_w^b$ and $\boldsymbol{\nabla}_w^b$ denote the noise of gyroscopes and accelerometers, respectively.

As stated above, the non-holonomic constraints can be regarded as virtual velocity measurements. From Equations (18) and (19), the two-dimensional measurement is formed as:

$$\mathbf{Z}_{\text{NHC}} = \begin{bmatrix} \tilde{v}_x^m \\ \tilde{v}_z^m \end{bmatrix} = \mathbf{M}_e^T \tilde{\mathbf{C}}_n^b \tilde{\mathbf{v}}_I^m \tag{25}$$

where $\mathbf{M}_e = [\mathbf{e}_1 \quad \mathbf{e}_3]$, in which \mathbf{e}_i is a unit three-dimensional column vector with the i th element being one.

The corresponding Kalman filter measurement equation is:

$$\mathbf{Z}_{\text{NHC}} = \mathbf{H}_{\text{NHC}} \mathbf{x} + \mathbf{V}_{\text{NHC}} \tag{26}$$

with \mathbf{V}_{NHC} denoting the measurement noise of NHC, and the measurement matrix is:

$$\mathbf{H}_{\text{NHC}} = [\mathbf{M}_1 \quad \mathbf{M}_2 \quad \mathbf{0}_{2 \times 9} \quad \mathbf{M}_3] \tag{27}$$

where $\mathbf{M}_1 = -\mathbf{M}_e^T \mathbf{C}_n^b (\mathbf{v}^n \times)$, $\mathbf{M}_2 = \mathbf{M}_e^T \mathbf{C}_n^b$, $\mathbf{M}_3 = -\mathbf{M}_e^T [(\mathbf{C}_n^b \mathbf{v}^n) \times] \mathbf{M}_e$.

2.3.3. *Observability of the error states.* Observability of the system is above all the first question to investigate, because if a state is unobservable, we have no way to achieve satisfactory estimation even with perfect measurements (Wu, 2014). Although an improved Kalman filter algorithm has been developed to accomplish the backtracking fine alignment, not all error states are observable under all conditions. In this section, we analyse the observability of the SINS/NHC integration filter depending on the system and measurement equations.

From Equation (21), the error equation is rearranged as:

$$\delta \tilde{\mathbf{v}}_I^m = \delta \tilde{\mathbf{v}}_I^b - \mathbf{v}^b \times \boldsymbol{\phi}^b - \mathbf{v}^b \times \boldsymbol{\alpha} \tag{28}$$

where $\delta \mathbf{v}_I^b = \mathbf{C}_n^b \delta \mathbf{v}_I^n$, $\mathbf{v}^b = \mathbf{C}_n^b \mathbf{v}^n$, $\boldsymbol{\phi}^b = \mathbf{C}_n^b \boldsymbol{\phi}^n$.

The measurement Equation (25) can be rewritten as:

$$\mathbf{Z}_{\text{NHC}} = \begin{bmatrix} \delta v_x^b - (\phi_z^b + \alpha_z)v_y^b \\ \delta v_z^b - (\phi_x^b + \alpha_x)v_y^b \end{bmatrix} \tag{29}$$

As time advances, the measurement values \mathbf{Z}_{NHC} and all-order derivatives can be treated as known quantities. According to the global observability theory (Wu et al., 2009), a state is said to be observable if it can be determined uniquely from the measurement equation for a finite time under a possible condition. From Equation (29), it can be seen that the measurement equation is irrelevant to position errors, so the position error states $\delta \mathbf{P}$ are obviously unobservable. Even so, the SINS/NHC integrated navigation can mitigate the drift of position errors by estimating the velocity errors.

Under static conditions, the longitudinal velocity v_y^b is zero, so the velocity error states δv_x^b and δv_z^b can be estimated but the forward velocity error δv_y^b is not directly observable in Equation (29). Assuming that the x_b axis of the IMU points to east, the observable velocity error δv_x^b corresponds to eastern velocity error δv_E , while when the x_b axis turns to north, δv_x^b corresponds to northern velocity error δv_N instead. So, the vertical velocity error is observable and the horizontal velocity errors can be alternatively estimated if the vehicle has a turning manoeuvre.

Due to the attitude errors and mounting angles, the observability of forward velocity δv_y^b cannot be directly decided from Equation (29) whether the vehicle is moving or not. Taking the derivative of Equation (28) with respect to time and considering the simplified velocity error equation $\delta \dot{\mathbf{v}}_{\text{INS}}^n \approx \mathbf{f}^n \times \boldsymbol{\phi}^n + \mathbf{C}_b^n \boldsymbol{\nabla}^b$, we get:

$$\begin{aligned} \delta \dot{\mathbf{v}}_I^b &= \dot{\mathbf{C}}_n^b \delta \mathbf{v}_I^n + \mathbf{C}_n^b \delta \dot{\mathbf{v}}_I^n - \dot{\mathbf{v}}^b \times \boldsymbol{\phi}^b - \mathbf{v}^b \times \dot{\boldsymbol{\phi}}^b - \dot{\mathbf{v}}^b \times \delta \boldsymbol{\alpha} \\ &\approx -\boldsymbol{\omega}_{nb}^b \times \delta \mathbf{v}_I^b + \mathbf{C}_n^b (\mathbf{f}^n \times \boldsymbol{\phi}^n + \boldsymbol{\nabla}^n) - \mathbf{C}_n^b (\mathbf{a}^n \times \boldsymbol{\phi}^n) - \mathbf{a}^b \times \delta \boldsymbol{\alpha} \\ &= -\boldsymbol{\omega}_{nb}^b \times \delta \mathbf{v}_I^b + \mathbf{C}_n^b [(\mathbf{f}^n - \mathbf{a}^n) \times \boldsymbol{\phi}^n + \boldsymbol{\nabla}^n] - \mathbf{a}^b \times \delta \boldsymbol{\alpha} \\ &= -\boldsymbol{\omega}_{nb}^b \times \delta \mathbf{v}_I^b - \mathbf{a}^b \times \delta \boldsymbol{\alpha} + \mathbf{C}_n^b (-\mathbf{g}^n \times \boldsymbol{\phi}^n + \boldsymbol{\nabla}^n) \end{aligned} \tag{30}$$

where $\mathbf{a}^b = [a_x^b, a_y^b, a_z^b]^T$ denotes acceleration in the b -frame, $\mathbf{a}^b = \dot{\mathbf{v}}^b$, $\mathbf{a}^n = \mathbf{C}_n^b \mathbf{a}^b$, $\boldsymbol{\phi}^b = \mathbf{C}_n^b \boldsymbol{\phi}^n$, $\boldsymbol{\nabla}^n = \mathbf{C}_b^n \boldsymbol{\nabla}^b$ and $\boldsymbol{\omega}_{nb}^b = [\omega_x, \omega_y, \omega_z]^T$ is the angular rate of the vehicle.

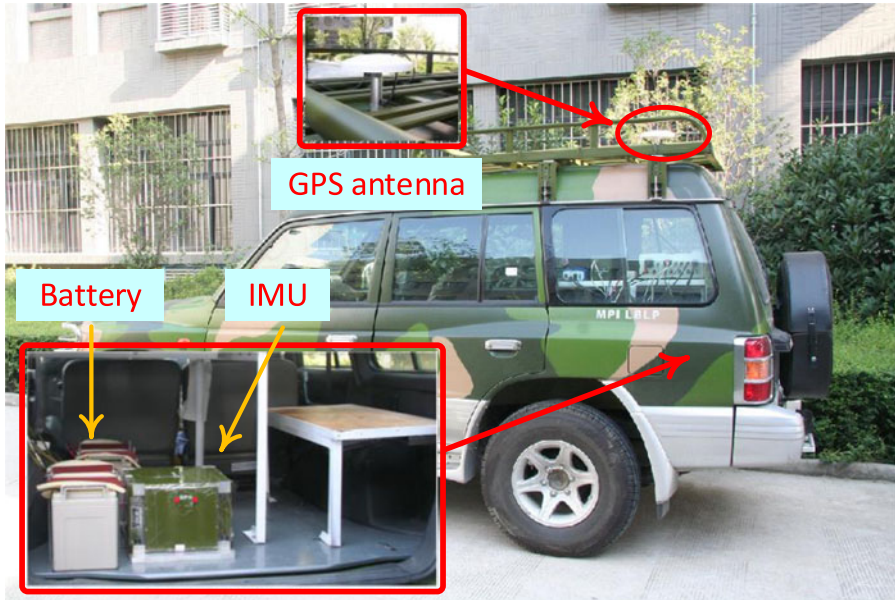


Figure 2. Experiment vehicle and equipment.

From Equation (30), the derivatives of measurement value satisfy:

$$\dot{Z}_{NHC} = \begin{bmatrix} \omega_z \delta v_y^b - \omega_y \delta v_z^b - a_y^b \alpha_z - g \phi_y^b + \nabla_x^b \\ \omega_y \delta v_x^b - \omega_x \delta v_y^b - a_x^b \alpha_x + \nabla_z^b \end{bmatrix} \tag{31}$$

As the left-hand side of Equation (31) can be treated as known quantities as time advances, the vertical acceleration bias ∇_z^b can be observed in a stationary state. Provided that there are sufficient turning manoeuvres, the azimuth rate ω_z will change while other coefficients remain constant, so the forward velocity error is solvable and thus observable. While the vehicle is accelerating or decelerating, the forward acceleration a_y^b is not zero and the mounting angles α_x, α_z are observable. Furthermore, the accelerometer bias ∇_x^b and level misalignments ϕ_E, ϕ_N can be further separated in angular motions when there is change of the attitude matrix.

The azimuth error ϕ_U has no effect in Equation (31) so it has lower observability. After the level misalignments and respective derivatives are solved, the azimuth angle error is determined by the attitude error equation of SINS:

$$\dot{\phi}^n \approx -\omega_{ie}^n \times \phi^n - \epsilon^n \tag{32}$$

It is obvious that the azimuth error is also estimated from the compass effect as stationary alignment, and the estimation accuracy is still restricted by the equivalent eastern gyro drift ϵ_E . So, angular excitation of a vehicle is helpful to improve the estimation accuracy of azimuth error by distinguishing the level gyro drifts ϵ_x^b and ϵ_y^b . In contrast to SINS/GPS integrated navigation, gyroscopes with higher accuracy are necessary for accurate positioning and orientation in the SINS/NHC integrated alignment filter.

Table 1. Specifications of the inertial sensors.

Gyroscope	Bias stability	0.007°/h
	Random Walk	0.001°/√h
Accelerometer	Bias stability	50 μg
	Random Walk	10 μg/√Hz

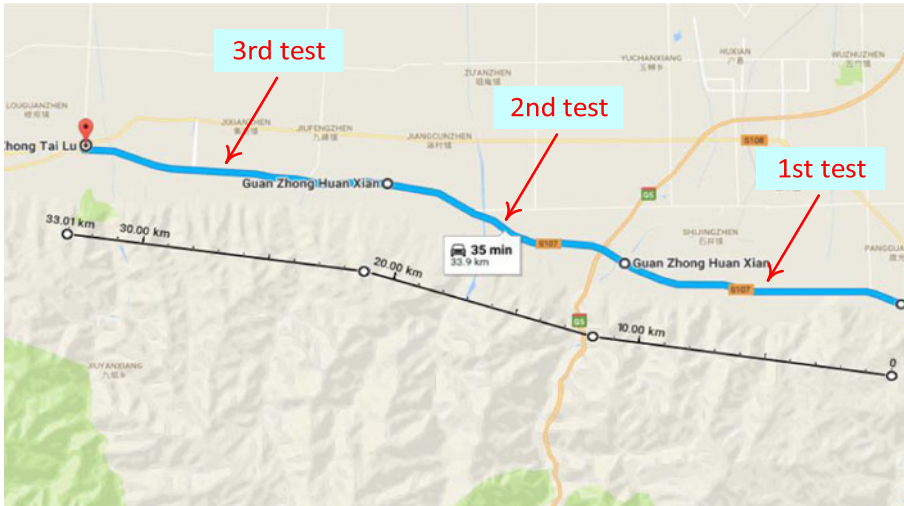


Figure 3. Trajectory along the country road during the experiment.

3. LAND VEHICLE IN-MOTION ALIGNMENT TESTS. In order to verify the performance of the proposed in-motion alignment method, three land vehicle tests were carried out. The land vehicle was equipped with a single-antenna GPS receiver and a navigation-grade Ring Laser Gyroscope (RLG) IMU with its axes roughly aligning with right, forward, upward directions of the vehicle, as shown in Figure 2.

The raw data update rate of the IMU was 200 Hz with its inertial sensors’ specifications listed in Table 1. A Novatel OEM615 GPS receiver with position accuracy of 1.5 m and velocity accuracy of 0.03 m/s was used as the position/velocity reference, while for attitude reference, a stationary-based initial alignment followed by SINS/GPS integrated navigation and Rauch-Tung-Striebel (RTS) post-smoothing (Simon, 2006) were conducted as the attitude reference.

The experimental procedure was designed as follows. Firstly, the car was kept stationary for about 10 minutes and the data was recorded to establish the attitude reference. Then three continuous in-motion alignments were carried out. As shown in Figure 3, we chose an extremely demanding scenario along a country road from east to west with few turns.

Figure 4 shows the travel speeds during the three tests. It can be seen that the alignment time of each test was about 10 minutes and the vehicle moved immediately when starting a mission. Having no external sensors, the in-motion alignment must start from the zero-speed state to obtain initial velocity information and the initial stationary time can be shortened to less than one second.

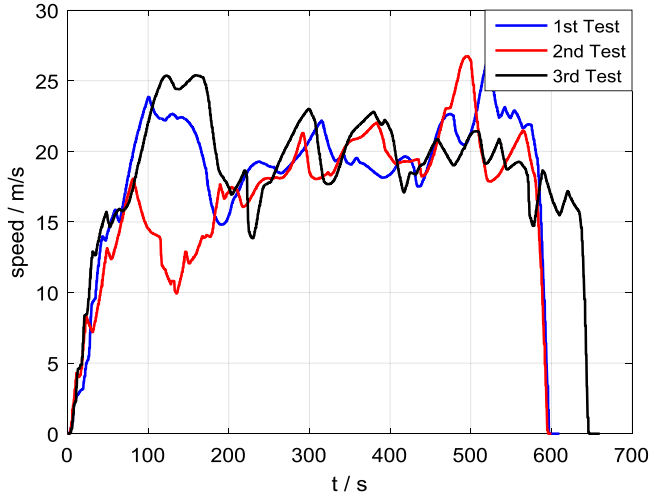


Figure 4. Travel speeds during the three vehicular tests.

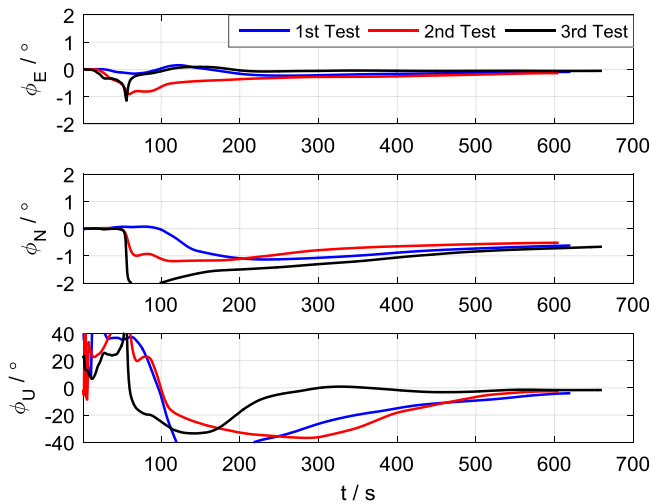


Figure 5. Attitude errors of the three DADCA.

As shown in [Figure 5](#), the attitude errors estimated by DADCA gradually converge with time. At the end of the DADCA process, the level misalignment angles are estimated accurately to within 1° and azimuthal misalignment angle to less than 4° , which meets the requirements of the subsequent linear fine alignment.

The attitude/velocity/position errors of the BFA processes with SINS/NHC integration are shown in [Figures 6–8](#), respectively. Due to the chosen east-west trajectory, the eastern velocity constraint is lacking most of the time, which leads to a larger eastern velocity error and northern misalignment than the other horizontal direction (northern velocity error and eastern misalignment).

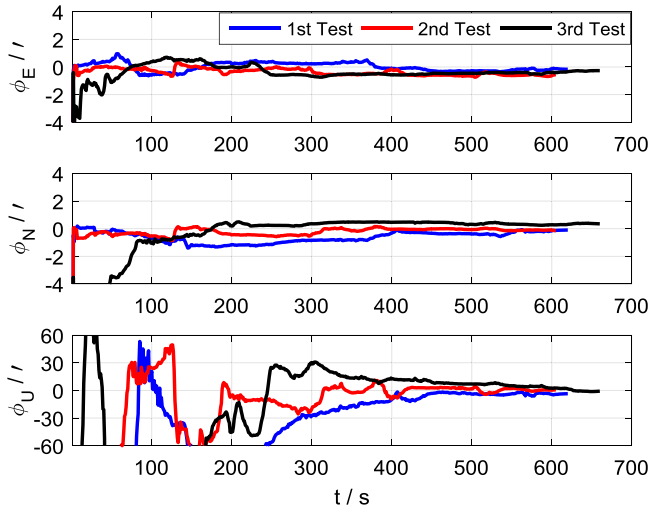


Figure 6. Attitude errors of BFA.

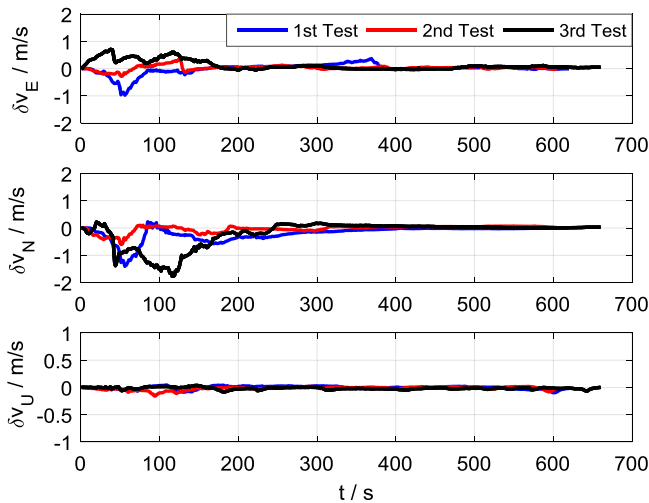


Figure 7. Velocity errors of BFA.

The Root Mean Square (RMS) statistic results at the end of the alignment are listed in Table 2. It can be seen that the azimuth alignment accuracy is 0.0358° (RMS) and the positioning accuracy is about 15 m (RMS). So, even without external auxiliary sensors, the proposed method can align the attitude to high accuracy and continuously determine the velocity and position with satisfactory accuracy.

The mounting angles estimated by the BFA process are given in Figure 9. Although the true mounting angles are unknown, the same convergence results in the three tests indicate the reliability of the estimation results. Affected by observability and manoeuvre conditions, the inertial sensor errors cannot be effectively estimated within a limited time apart from the vertical accelerometer bias. This is not a big problem for a navigation-grade

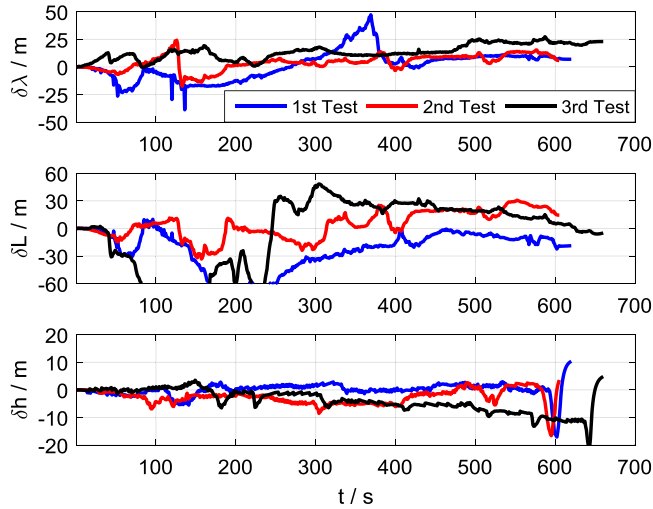


Figure 8. Position errors of BFA.

Table 2. RMS errors of BFA.

	East	North	Up
Attitude ($^{\circ}$)	0.00375	0.00615	0.0358
Velocity (m/s)	0.028	0.019	0.017
Position (m)	14.27	13.97	6.93

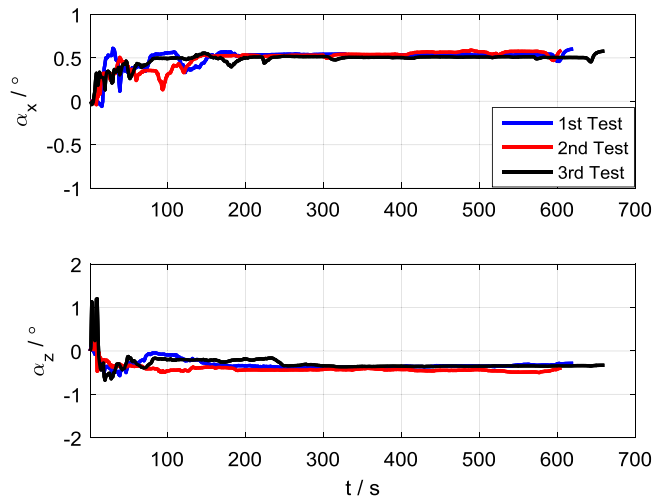


Figure 9. Mounting angles estimated by BFA.

SINS with the capability of self-alignment. Given sufficient accuracy of the gyroscopes and accelerometers, satisfactory in-motion alignment accuracy can be obtained by the proposed method.

4. CONCLUSION. The proposed alignment scheme in this paper does not rely on any external sensors to realise accurate in-motion alignment for land vehicle SINS. Once the initial position is available, the vehicle can move immediately, and accurate attitude, position and velocity information can be determined within a given alignment time. Three vehicle tests were carried out along an east-west country road, and the results show that the azimuth alignment accuracy is 0.0358° (RMS) and the positioning errors is about 15 m (RMS). The proposed method here may also be suitable for velocity-aided or position-aided in-motion alignment in other applications such as aviation and marine.

REFERENCES

- Bimal Raj, K. and Joshi, A. (2015). In-motion alignment of inertial navigation system with doppler speed measurements. *AIAA Guidance, Navigation, and Control Conference*, Kissimmee, FL.
- Chang, L., He, H. and Qin, F. (2016). In-Motion Initial Alignment for Odometer-Aided Strapdown Inertial Navigation System Based on Attitude Estimation. *IEEE Sensors Journal*, **17**(3), 766–773.
- Chang, L., Li, Y. and Xue, B. (2017). Initial Alignment for a Doppler Velocity Log-Aided Strapdown Inertial Navigation System With Limited Information. *IEEE/ASME Transactions on Mechatronics*, **22**(1), 329–338.
- Dissanayake, G., Sukkarieh, S., Nebot, E. and Whyte, H. D. (1999). A new algorithm for the alignment of inertial measurement units without external observation for land vehicle applications. *IEEE International Conference on Robotics and Automation, 1999. Proceedings. IEEE, 1999*, Detroit, MI.
- Dissanayake, G., Sukkarieh, S., Nebot, E. and Whyte, H. D. (2001). The aiding of a low-cost strapdown inertial measurement unit using vehicle model constraints for land vehicle applications. *IEEE transactions on robotics and automation*, **17**(5), 731–747.
- Fu, Q. W., Qin, Y. Y., Li, S. H. and Wang, H. M. (2012). Inertial navigation algorithm aided by motion constraints of vehicle. *Journal of Chinese Inertial Technology*, **20**(6), 640–643.
- Gu, D., El-Sheimy, N., Hassan, T. and Syed, Z. (2008). Coarse alignment for marine SINS using gravity in the inertial frame as a reference. *Position, Location and Navigation Symposium, 2008 IEEE/ION*, Monterey, CA.
- Hu, J. and Cheng, X. (2014). A new in-motion initial alignment for land-vehicle SINS/OD integrated system. *IEEE/ION Position, Location and Navigation Symposium - PLANS 2014*, Monterey, CA.
- James, R.W. (2012). *Spacecraft attitude determination and control*. Springer Science & Business Media.
- Jiang, Y. F., Xie, B. and Weng, J. (2013). SINS in-motion alignment and position determination for land-vehicle based on quaternion Kalman filter. *Control Conference (CCC), 2013 32nd Chinese*, Xi'an, China.
- Jiang, Y. F. (1998). Error analysis of analytic coarse alignment methods. *IEEE Transactions on Aerospace and Electronic Systems*, **34**(1), 334–337.
- Kaygisiz, B. H. and Şen, B. (2015). In-motion alignment of a low-cost GPS/INS under large heading error. *The Journal of Navigation*, **68**(2), 355–366.
- Kubo, Y., Fujioka, S., Nishiyama, M. and Sugimoto, S. (2006). Nonlinear filtering methods for the INS/GPS in-motion alignment and navigation. *International Journal of Innovative Computing, Information and Control*, **2**(5), 1137–1151.
- Li, W., Tang, K., Lu, L. and Wu, Y. (2013a). Optimization-based INS in-motion alignment approach for underwater vehicles. *Optik - International Journal for Light and Electron Optics*, **124**(20), 4581–4585.
- Li, W., Wang, J., Lu, L. and Wu, W. (2013b). A Novel Scheme for DVL-Aided SINS In-Motion Alignment Using UKF Techniques. *Sensors*, **13**(1), 1046.
- Li, W., Wu, W. and Lu, J. W. L. (2013c). A Fast SINS Initial Alignment Scheme for Underwater Vehicle Applications. *Journal of Navigation*, **66**(2), 181–198.
- Li, W., Wu, W., Wang, J. and Wu, M. (2014). A novel backtracking navigation scheme for Autonomous Underwater Vehicles. *Measurement*, **47**(47), 496–504.
- Liu, T., Xu, Q. and Li, Y. (2014). Adaptive filtering design for in-motion alignment of INS. *26th Chinese Control and Decision Conference, CCDC*, Changsha., China.
- Liu, Y., Li, S., Fu, Q., and Liu, Z. (2018). Impact Assessment of GNSS Spoofing Attacks on INS/GNSS Integrated Navigation System. *Sensors*, **18**(5), Article 1433.
- Pan, X. and Wu, Y. (2016). Underwater Doppler Navigation with Self-calibration. *Journal of Navigation*, **69**(2), 295–312.

- Peng, K. Y., Lin, C. A. and Chiang, K. W. (2013). Performance analysis of an AKF based tightly-coupled INS/GNSS integrated scheme with NHC for land vehicular applications. *Transactions- Canadian Society for Mechanical Engineering*, **37**(3):503–513.
- Qin, Y. Y. (2014). *Inertial Navigation, 2nd Edition*. China Science Press.
- Rothman, Y., Klein, I. and Filin, S. (2015). Analytical Observability Analysis of INS with Vehicle Constraints. *Navigation*, **61**(3):227–236.
- Savage, P. G., (2000). *Strapdown Analytics, 2nd*. Strapdown Associates, Inc.
- Shin, E. H. and El-Sheimy, N. (2004). An unscented Kalman filter for in-motion alignment of low-cost IMUs. *IEEE/ION Position, Location and Navigation Symposium - PLANS 2004*, Monterey, CA.
- Silson, P. M. G. (2011). Coarse Alignment of a Ship's Strapdown Inertial Attitude Reference System Using Velocity Loci. *IEEE Transactions on Instrumentation & Measurement*, **60**(6), 1930–1941.
- Simon, D. (2006). *Optimal state estimation: Kalman, H infinity, and nonlinear approaches*. John Wiley & Sons.
- Titterton, D. H. and Weston, J. L. (2004). *Strapdown inertial navigation technology, 2nd*. Institution of Electrical Engineers.
- Wang, Q, Fu, M., Xiao, X. and Deng, Z. (2012). Automatic calibration and in-motion alignment of an odometer-aided INS. *Proceedings of the 31st Chinese Control Conference, CCC*, Hefei, China.
- Wu, M., Wu, Y., Hu, X. and Hu, D. (2011). Optimization-based alignment for inertial navigation systems: Theory and algorithm. *Aerospace Science and Technology*, **15**(1), 1–17.
- Wu, Y. and Pan, X. (2013a). Velocity/position integration formula part I: Application to in-flight coarse alignment. *IEEE Transactions on Aerospace and Electronic Systems*, **49**(2), 1006–1023.
- Wu, Y. and Pan, X. (2013b). Velocity/position integration formula part II: application to strapdown inertial navigation computation. *IEEE Transactions on Aerospace and Electronic Systems*, **49**(2), 1024–1034.
- Wu, Y., Wu, M., Hu, X. and Hu, D. (2009). Self-calibration for land navigation using inertial sensors and odometer: Observability analysis. *AIAA Guidance, Navigation, and Control Conference and Exhibit, 2009*, Chicago, IL.
- Wu, Y. (2014). Versatile land navigation using inertial sensors and odometry: Self-calibration, in-motion alignment and positioning. *Inertial Sensors and Systems Symposium (ISS), 2014 DGON*, Karlsruhe, Germany.
- Xu, J., He, H., Qin, F. and Chang, L. (2017). A Novel Autonomous Initial Alignment Method for Strapdown Inertial Navigation System. *IEEE Transactions on Instrumentation and Measurement*, **66**(9), 2274–2282.